Research Article Open Access

Haoliang Qian†, Yuzhe Xiao†, Dominic Lepage†, Li Chen, and Zhaowei Liu*

Quantum Electrostatic Model for Optical Properties of Nanoscale Gold Films

DOI 10.1515/nanoph-2015-0022
Received July 27, 2015; accepted September 11, 2015

Abstract: The optical properties of thin gold films with thickness varying from 2.5 nm to 30 nm are investigated. Due to the quantum size effect, the optical constants of the thin gold film deviate from the Drude model for bulk material as film thickness decreases, especially around 2.5 nm, where the electron energy level becomes discrete. A theory based on the self-consistent solution of the Schrödinger equation and the Poisson equation is proposed and its predictions agree well with experimental results.

Keywords: ultrathin gold film; quantum plasmonics; metal quantum well; optical property

1 Introduction

Plasmonics, which utilizes the interaction of light and charged particles, such as electrons in metals, has been an area of interest for decades. It has led to many fascinating applications, such as super-resolution imaging that breaks the diffraction limit [1, 2], new kinds of biosensors with enhanced performance [3, 4], nanolasers [5], and optical metamaterials that can manipulate light–matter interaction in a unknown degree of freedom [6, 7]. With the development of nanofabrication techniques, the dimensions of the plasmonic device have been shrunk to the nanoscale [8]. To understand and explore the physics within such small plasmonic devices, quantum confinement effects need to be considered. In this context, the field of quantum plasmonics, which combines quantum mechanics with plasmonics, has emerged and drawn much attention recently [9, 10]. There have been several approaches to deal with quantum plasmonics, for example, nanoparticles with quantum size model [11], quantum correlated model [12], and nonlocal model [13, 14]. Here, we choose the ultrathin metal film as a platform to study quantum plasmonics and focus on the optical properties of the nanoscale gold film. We experimentally measure the reflection and transmission (RT) of thin gold films with thicknesses varying from 30 nm to 2.5 nm, and then extract the optical constants. It is found that the optical properties of thin gold film show significant difference when the film thickness decreases, especially around 2.5 nm. With such small thickness, a metal quantum well with discrete energy levels is formed, and the behavior of the electrons inside would mainly be governed by quantum physics.

Although the quantum behavior has been extensively explored with various theoretical models in the context of semiconductor quantum wells [15], these models cannot be directly applied to metals, due to the large electron density and different band structures. Thin metal films had previously drawn wide research interest in the context of quantum physics [16–19], and recent effort has been focused on the optical properties of ultrathin metal films with thickness of a few nanometers [20–26]. Besides the classical Drude model [27], several new theoretical methods have been proposed, such as the quantum size model [11, 21] and density function theory [26]. The agreement between those theoretical models and experimental result, however, is only qualitative, and a more accurate model is still not available according to our knowledge. Therefore, we propose a new model, which we call the quantum electrostatic model (QEM) to study electron dynamics within a metal quantum well. More specifically, a theory based on the self-consistent solution of the Schrödinger equation and the Poisson equation is applied to thin gold films, and its predictions agree well with experimental results.

***Corresponding Author: Zhaowei Liu:** Department of Electrical and Computer Engineering, University of California, San Diego, 9500 Gilman Dr, La Jolla, CA, USA 92093; Material Science and Engineering, University of California, San Diego, 9500 Gilman Dr, La Jolla, CA, USA 92093; Center for Magnetic Recording Research, University of California, San Diego, 9500 Gilman Dr, La Jolla, CA, USA 92093; E-mail: zhaowei@ucsd.edu
Haoliang Qian†, Yuzhe Xiao†, Dominic Lepage†: Department of Electrical and Computer Engineering, University of California, San Diego, 9500 Gilman Dr, La Jolla, CA, USA 92093; These authors contributed equally to this work
Li Chen: Center for Magnetic Recording Research, University of California, San Diego, 9500 Gilman Dr, La Jolla, CA, USA 92093
† These authors contributed equally in this work.

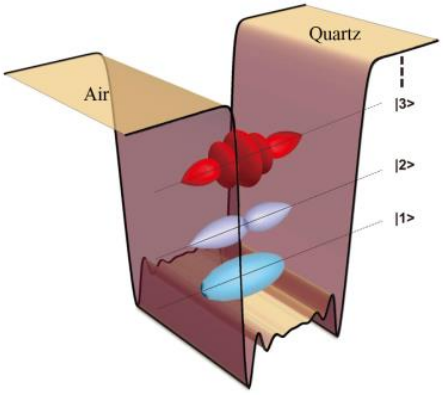

Figure 1: A metal quantum well structure is formed based on an ultrathin gold film sandwiched between the quartz substrate and air on top. The first three lowest energy levels and their corresponding wave functions are also sketched. The shape deformation of the well bottom indicates the impact of electron distribution.

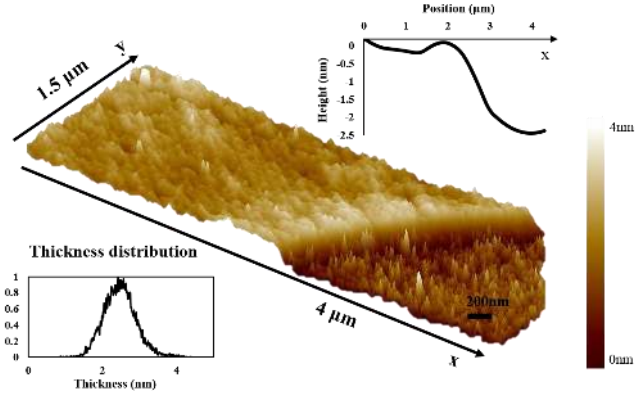

Figure 2: Atomic-force microscopy image of one of the 2.5 nm thin gold films, showing the film edge on the substrate. The upper inset shows the averaged height on both sides across the edge (the mean thickness), indicating the mean thickness of the film is about 2.5 nm. The lower inset shows the surface roughness is around 0.5 nm.

2 Results And Discussion

Thin gold film is grown (see Supplementary Material for fabrication details) on top of a quartz substrate. The quantum confinement effects become pronounced when the thickness of the film is comparable to the de Broglie wavelength of the electron. For ultrasmall thickness, a quantum well would be formed by the potential barrier from air and quartz on two sides of the gold, and the initial continuum energy levels of the free electrons become discrete in the quantum well. The band structure of the metal quantum well, and the three lowest eigen energy levels together with their wave functions are schematically sketched in Figure 1. The optical properties of such quantum sized metal films represent an overall collective effect of the dynamics of the quantized electrons within the quantum well, and hence would be drastically different from the free electron gas model applied in bulk metals.

Figure 2 shows the atomic-force microscopy (AFM) image of a 2.5 nm gold film sample. As can be seen, although the film is not perfectly flat as indicated by the surface fluctuations, it is not broken at the 2.5 nm thickness level. (A better resolution scanning for a small area is shown in Figure S1 in Supplementary Material). The averaged height shown in the upper inset indicates that the average thickness of the film is about 2.5 nm. Also shown in the lower inset is the statistics of the film thickness variations, where we can see the surface roughness (root mean square) of the film thickness is about 0.5 nm, which is also the typical surface roughness for thicker films.

To characterize the optical properties of our thin film samples, RT measurements are performed using the commercialized spectrophotometer Lambda 1050 system with different incident angles and polarizations for different film thicknesses. The measured RT curves with 45 degree incident angle and P-polarization for 2.5 nm, 7 nm, and 30 nm films are plotted in Figure 3(a) and 3(b), respectively. (Experimental data for different incident angles and polarizations is provided in Section 5 in Supplementary Material). As can be seen from Figure 3(b), the transmission curves for 7 and 30 nm thick samples behave quite similarly and they decrease monotonically as wavelength increases. The 2.5 nm thick sample, however, exhibits a distinct behavior: its transmission increases slightly with wavelength. Reflection curves of the 2.5 nm films also show significantly different behavior compared with the thicker ones, as shown in Figure 3(a).

Optical constants for these thin film samples can be extracted from the measured RT curves in Figure 3(a) and 3(b). In order to extract the refractive index n and extinction coefficient k, an extraction strategy is developed, which combines a multilayer transfer matrix method [28] and a two-dimensional Newton iteration method. More details of this strategy are provided in Supplementary Material. The corresponding extracted n and k values for films with different thicknesses are plotted in Figure 3(c) and 3(d), respectively. Also the n and k values for bulk gold from John and Christy [27] are plotted using black dashed curves. Both n and k values for 7 nm and 30 nm are quite similar and converge to bulk values, which is expected. The case of the 2.5 nm film is quite different: the refractive index n is significantly larger, while the extinction coefficient k is much smaller than the bulk value. The increase of n and the decrease of k make the 2.5 nm gold film less like a metal. Moreover, unlike the n and k for thicker films (where both increase with wavelength), n decreases, while

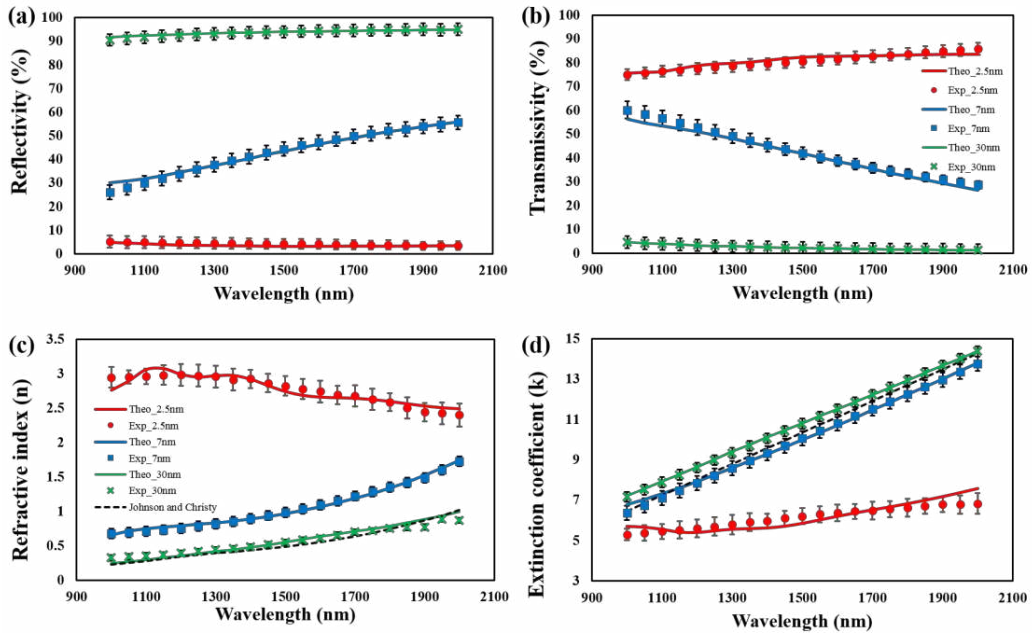

Figure 3: Reflection (a) and transmission (b) with refractive index n (c) and extinction coefficient k (d) for the 2.5 nm, 7 nm, and 30 nm samples. Optical constants of the thin film samples are extracted from RT data. n and k for 7 nm and 30 nm are very similar, and converge to bulk values (dashed line, tabulated data from John and Christy [27]). The behavior for the 2.5 nm sample is significantly different from those for 7 and 30 nm samples, indicating the impact of quantum size effect. Predictions from our QEM are also plotted, all showing good agreement with the experimental result.

k increases with wavelength for 2.5 nm film in the 1 to 2 μm wavelength range.

Clearly, such a distinct behavior of the optical constants is related to the change in film thickness. In order to investigate the optical properties of our metal quantum well samples, we propose a QEM to characterize the electron dynamics within thin metal films, in which the starting point is the Schrödinger equation:

$$\frac{1}{2m}\left[\hat{\vec{p}} + \frac{e}{c}\vec{A}\right]^2 |\varphi\rangle + V(\vec{r})\,|\varphi\rangle + \phi(\vec{r})\,|\varphi\rangle = E\,|\varphi\rangle\,, \quad (1)$$

where m and e are the effective mass and charge of the free electrons, $\hat{\vec{p}}$ is the momentum operator, c is the speed of light in vacuum, $\vec{A}$ and $\phi\left(\vec{r}\right)$ are the vector and scalar potentials associated with the applied electromagnetic field, which are set to be zero in our case, and $V\left(\vec{r}\right)$ is the potential determined by the quantum well structure.

The solution from the Schrödinger equation alone, however, is not self-consistent because the potential $V\left(\vec{r}\right)$ is modified by the electron distribution inside the quantum well. To account for this effect, the Poisson equation needs to be included. The coupled Schrödinger–Poisson equation approach has been considered in a study for semiconductor quantum wires [29], but this method cannot be directly applied to metal, because of hard convergence induced by the larger electron density with different band structures. For this purpose, a modified iteration scheme for the coupled Schrödinger–Poisson equation is developed here for metal quantum wells. (See Supplementary Material for iteration method details.) First, the Schrödinger equation is solved with an initial value for the potential $V\left(\vec{r}\right)$ from the shape of the quantum well. Electron density is then obtained from the eigen energies E_k and wave functions φ_k following

$$\rho(z) = \sum_{k=1} \left|\varphi_k(z)\right|^2 \frac{m}{\pi\hbar^2} \int_{E_k}^{\infty} \frac{dE}{1 + e^{(E-\mu)/k_B T}}, \quad (2)$$

where μ is the Fermi energy, $\hbar$ is the reduced Planck constant, k_B is the Boltzmann constant, T is the kelvin temperature, and we assume the quantum well is in the z direction. The Poisson equation is then solved to find the new potential $V\left(\vec{r}\right)$ based on the electron density calculated from Eq. (2):

$$\nabla\left[\varepsilon_0 \varepsilon_{static} \nabla V(z)\right] = -\rho(z), \quad (3)$$

where ε_0 is the vacuum permittivity and ε_{static} is the relative static permittivity of the gold film. The updated potential $V(z)$ is then substituted back into the Schrödinger equation to solve for the new eigen energies and wave functions. This iteration process is repeated until finally a self-consistent electron density $\rho(z)$ and potential $V(z)$ are obtained.

Table 1: Simulation parameters for the 2.5 nm, 7 nm, and 30 nm thick thin films.

Thickness (nm)	m	τ (fs)	ε_{static}
2.5	~$0.36m_e$	~4.54	~−1300
7	~$0.81m_e$	~7.05	~−7000
30	~m_e	~10	~−15000

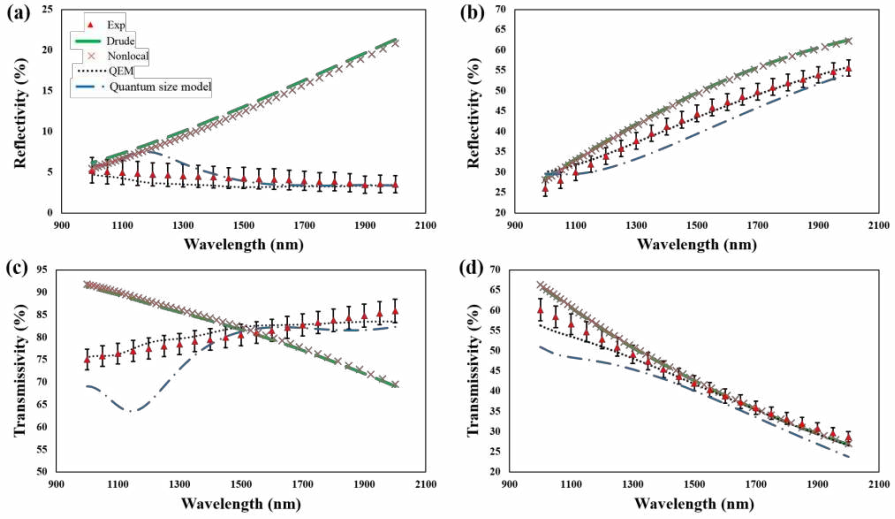

Figure 4: Comparison between reflection (top) and transmission (bottom) for 2.5 nm (a and c) and 7 nm (b and d) gold films for which the refractive index n and k are from the Drude model, nonlocal model, quantum size model, and quantum electrostatic model. The corresponding experimental results are marked by red triangles.

Once the eigen energy E_n and eigen wave function $|\varphi_n\rangle$ are solved from the iteration process, the permittivity of the metal quantum well can be calculated using the following expression [11]:

$$\varepsilon = 1 - \frac{\omega_p^2}{\omega^2} - \frac{8\pi e^2}{\Omega m^2 \omega^2} \sum_{ij} \frac{f_i E_{ij} \left| \left\langle i \left| \hat{\vec{p}} \right| j \right\rangle \right|^2}{E_{ij}^2 - \hbar^2 \omega^2}, \qquad (4)$$

where the plasma frequency ω_p is determined by the electron density ρ_e through $\omega_p^2 = \rho_e e^2/m\varepsilon_0$, Ω is the volume of the quantum well, $E_{ij} = E_i - E_j$ is the difference in eigen energies, and $f_i = 1/(1 + e^{(E_i-\mu)/k_BT})$ is the Fermi–Dirac occupation factor for the i_{th} state.

The above iteration assumes a quantum well from a perfect metal film, where the relaxation process of electrons is neglected. In reality, electrons are affected by the relaxation process due to either lattice vibration (thermal excitations), or static imperfections (such as impurities) or the impact of boundaries [30]. So it is necessary to include this effect as well. An electron relaxation time τ is used to quantify the strength of this effect. Such an effect cannot be included simply by replacing ω with $\omega + i/\tau$ in Eq. (4) because it fails to conserve the local electron number [31]. In order to account for the relaxation process, we adopted the model from Mermin [31], and the permittivity is obtained in the following form:

$$\varepsilon_{corr}(\omega) = 1 + \frac{(1 + i/\omega\tau)(\varepsilon - 1)}{1 + (i/\omega\tau)(\varepsilon - 1)/(\varepsilon_{static} - 1)}. \qquad (5)$$

The refractive index n and extinction coefficient k are finally obtained as: $n = \mathrm{Re}\{\sqrt{\varepsilon_{corr}}\}$ and $k = \mathrm{Im}\{\sqrt{\varepsilon_{corr}}\}$.

Numerical simulations based on the QEM are performed for our thin metal films with different thicknesses. The corresponding RT curves for the calculated n and k values are plotted in Figure 3, where theoretical predictions match quite well with experimental results for all three different thickness samples from the bulk property metal to the metal quantum well. This clearly shows that QEM is valid in describing the electron dynamics inside a metal quantum well. The reason for such different behavior for the 2.5 nm thin film as compared to the thicker ones (7 nm and 15 nm) is the modification of the quantum-corrected term (the last term on the right-hand side of Eq. (4)) to the material property. In the limit of the bulk gold film, the energy states of the "free" electrons are a continuum and the wave functions are plane waves, which leads the quantum-corrected term to go to zero. The contribution from this term is no longer zero in the quantum re-

gion, where the "free" electrons are quantized. The quantization makes this material system behave less like a metal, which can also be found from the permittivity of the 2.5 nm film (see Figure S5 in Supplementary Material).

It is important to note that our model characterizes the behavior of free electrons under the impact of quantum size effect. It can be applied to materials as long as their electron properties can be approximated by the free electron model, and can be very easily generalized to other metallic quantum structures, such as quantum wires and quantum dots. Other effects that are related to the band structure of the gold atom itself, such as the interband transition and exciton absorption, are not covered in this model, but can be included by adding the additional terms. For example, the interband transition can be included through $\varepsilon = \varepsilon_{corr} + \varepsilon_{IB}$, where the ε_{IB} represents the interband transition [32]. Full n, k data from 500 nm to 2 μm and further discussion on the impact of interband tranisition [27] for the wavlength range below 1 μm are provided in Supplementary Material.

The parameters used in our numerical simulations for the 30 nm, 7 nm, and 2.5 nm thick films are summarized in Table 1. As shown in Table 1, the parameters of 30 nm samples are almost identical to those of the bulk material, which is expected. As film thickness is reduced, the electron effective mass m, relaxation time τ, and the absolute value of static permittivity ε_{static} all decrease. The reduction of the relaxation time agrees with previous investigation [30, 33], and can be understood from the fact that the impact of boundaries and imperfection from thickness variation becomes more and more important as film thickness is reduced. The effective mass of thin gold film was experimentally measured to be smaller than its bulk value previously [34, 35]. The static permittivity has been investigated for thin films and was also found to decrease as thickness is reduced [36, 37]. All parameters are in a reasonable range and agree with previous findings.

As a final comparison, we plot the calculated RT curves from the Drude model, nonlocal model, quantum size model, and QEM with 2.5 nm and 7 nm gold films, together with the measured experimental curves in Figure 4. For the Drude model, we use a plasma frequency $\omega_p = 1.38 \times 10^{16}$ rad/s and relaxation time $\tau = 9.3$ fs, which are the typical values for gold. For the nonlocal model, we adopt the model from Ref. [13] and use the parameters for gold provided therein. For the quantum size model, we use the model from Ref. [11] and the same parameters listed in Table 1. As can be seen from Figure 4, the Drude model can give reasonably good predictions of RT curves for the 7 nm sample, where the quantum effect is not so pronounced. As the thickness reduces down to 2.5 nm, clear discrepancy can be seen between the Drude model and the experiment. Also, it is found that the ultrathin gold film has a quite weak nonlocal effect, and the nonlocal calculation shows negligible difference as compared to the Drude model. For the quantum size model, good prediction has been found in the long wavelength region ($\lambda > 1.4$ μm), but considerable disagreement shows up at shorter wavelengths for a 2.5 nm thin film. Instead, our QEM has excellent agreement with experimental results for both 7 nm and 2.5 nm samples in a broad range of wavelengths. Figure 4 clearly implies that QEM, which considers the quantum confinement effect together with the impact of self-consistent electron redistribution, should be used for the case of metal quantum well structures.

3 Conclusion

To summarize, we have proposed an iterative quantum model to deal with electron dynamics within a metal quantum well. We investigate this quantum plasmonic effect by studying the impact of quantum size effects on the optical properties of thin metal films. Reflection and transmission curves are measured; refractive index n and extinction coefficient k are extracted for films with different thicknesses. Our QEM can explain the experimental results quite well. Such a theory can also be generalized to other quantum structures, and would be very useful in the field of quantum plasmonics.

4 Method

Fabrication methods

The commercial sputtering machine AJA International is used for thin gold film growth and the qualities of the thin gold film samples are calibrated by two kinds of methods. For the 30 nm gold film, we use X-ray diffraction (XRD) for calibration. For the 2.5 nm thin gold film, AFM is needed for obtaining the information regarding the surface roughness and film thickness.

Measurement system

Reflection and transmission measurements are performed using the commercialized spectrophotometer Lambda 1050 system with different incident angles and polarizations for different film thicknesses.

Acknowledgement: The authors thank Conrad Rizal for help with XRD measurement, and Lorenzo Ferrari, Yaoguang Ma, and Conor Riley for help with RT measurement. The authors acknowledge financial support from the Office of Naval Research (ONR) Young Investigator Award (Grant No. N00014-13-1-0535) and the Defense Advanced Research Projects Agency (DARPA) Young Faculty Award (Grant No. D13AP00054).

Bibliography

[1] J.B. Pendry, Phys Rev Lett 85, 3966 (2000).
[2] Z.W. Liu, H. Lee, Y. Xiong, C. Sun, and X. Zhang, Science 315, 1686 (2007).
[3] J.N. Anker, W.P. Hall, O. Lyandres, N.C. Shah, J. Zhao, and R.P. Van Duyne, Nat Mater 7, 442 (2008).
[4] A.G. Brolo, Nat Photonics 6, 709 (2012).
[5] M. Khajavikhan, A. Simic, M. Katz, J.H. Lee, B. Slutsky, A. Mizrahi, V. Lomakin, and Y. Fainman, Nature 482, 204 (2012).
[6] W. Cai and V. Shalaev, Optical Metamaterials: Fundamentals and Applications, 1 (2010).
[7] I.V. Shadrivov, P.V. Kapitanova, S.I. Maslovski, and Y.S. Kivshar, Phys Rev Lett 109, 083902 (2012).
[8] M.I. Stockman, Opt Express 19, 22029 (2011).
[9] J.A. Scholl, A.L. Koh, and J.A. Dionne, Nature 483, 421 (2012).
[10] M.S. Tame, K.R. McEnery, S.K. Ozdemir, J. Lee, S.A. Maier, and M.S. Kim, Nat Phys 9, 329 (2013).
[11] D.M. Wood and N.W. Ashcroft, Phys Rev B 25, 6255 (1982).
[12] R. Esteban, A.G. Borisov, P. Nordlander, and J. Aizpurua, Nat Commun 3, 825 (2012).
[13] N.A. Mortensen, S. Raza, M. Wubs, T. Sondergaard, and S.I. Bozhevolnyi, Nat Commun 5, 3809 (2014).
[14] Y. Luo, A.I. Fernandez-Dominguez, A. Wiener, S.A. Maier, and J.B. Pendry, Phys Rev Lett 111, 093901 (2013).
[15] S. Schmittrink, D.S. Chemla, and D.A.B. Miller, Adv Phys 38, 89 (1989).
[16] N. Trivedi and N.W. Ashcroft, Phys Rev B 38, 12298 (1988).
[17] J.J. Paggel, T. Miller, and T.C. Chiang, Science 283, 1709 (1999).
[18] M. Milun, P. Pervan, and D.P. Woodruff, Rep Prog Phys 65, 99 (2002).
[19] W.B. Su, C.S. Chang, and T.T. Tsong, J Phys D Appl Phys, 013001 43 (2010).
[20] J. Szczyrbowski, J. Dryzek, and A. Czapla, Thin Solid Films 112, 175 (1984).
[21] J. Dryzek and A. Czapla, Phys Rev Lett 58, 721 (1987).
[22] I.V. Antonets, L.N. Kotov, S.V. Nekipelov, and E.N. Karpushov, Tech Phys+ 49, 1496 (2004).
[23] X.F. Wang, K.P. Chen, M. Zhao, and D.D. Nolte, Opt Express 18, 24859 (2010).
[24] J. Siegel, O. Lyutakov, V. Rybka, Z. Kolska, and V. Svorcik, Nanoscale Res Lett 6, 96 (2011).
[25] A. Axelevitch, B. Gorenstein, and G. Golan, Physcs Proc 32, 1 (2012).
[26] S. Laref, J. Cao, A. Asaduzzaman, K. Runge, P. Deymier, R.W. Ziolkowski, M. Miyawaki, and K. Muralidharan, Opt Express 21, 11827 (2013).
[27] P.B. Johnson and R.W. Christy, Phys Rev B 6, 4370 (1972).
[28] P. Yeh, A. Yariv, and C.S. Hong, J Opt Soc Am 67, 423 (1977).
[29] A. Trellakis, A.T. Galick, A. Pacelli, and U. Ravaioli, J Appl Phys 81, 7880 (1997).
[30] R.P. Feynman, Found Phys 16, 507 (1986).
[31] N.D. Mermin, Phys Rev B-Solid St 1, 2362 (1970).
[32] P.G. Etchegoin, E.C. Le Ru, and M. Meyer, J Chem Phys 125, 164705 (2006).
[33] A.V. Lugovskoy and I. Bray, Phys Rev B 65, 045405 (2002).
[34] R.C. Jaklevic and J. Lambe, Phys Rev B 12, 4146 (1975).
[35] N. Nilius, T.M. Wallis, and W. Ho, Science 297, 1853 (2002).
[36] J.J. Tu, C.C. Homes, and M. Strongin, Phys Rev Lett 90, 017402 (2003).
[37] M. Hovel, B. Gompf, and M. Dressel, Phys Rev B 81, 035402 (2010).

Supplemental Material: The online version of this article (DOI: 10.1515/nanoph-2015-0022) offers supplementary material.